



A Review on Li⁺/H⁺ Exchange in Garnet Solid Electrolytes: From Instability against Humidity to Sustainable Processing in Water

Ruijie Ye,^[a, b] Martin Ihrig,^[a] Nobuyuki Imanishi,^[c] Martin Finsterbusch,^{*,[a, d]} and Egbert Figgemeier^{*,[b, d]}

Garnet-based Li-ion conductors are one of the most promising oxide-ceramic solid electrolytes for next-generation Li batteries. However, they undergo a Li⁺/H⁺ exchange (LHX) reaction with most protic solvents used in component manufacturing routes and even with moisture in ambient air. These protonated garnets show a lower Li-ionic conductivity, and even if only the surface is protonated, this degraded layer hinders the Li-ion exchange with, for example, a metallic Li anode. Furthermore, the resulting unstable surface properties during the processing in air lead to challenges with respect to reproducibility of the final component performance, limiting their commercial applic-

ability. However, in recent years, the knowledge about the underlying chemical mechanisms has led to the development of mitigation strategies and enabled a push of this promising material class towards sustainable and scalable fabrication routes. This Minireview covers the following four aspects, which are relevant for a comprehensive understanding of these developments: (1) reports of LHX phenomenon in garnets exposed to air and solvents; (2) recent understandings of the fundamentals and properties of LHX; (3) strategies to prevent LHX and to recover garnets; and (4) sustainable application of LHX for material processing and energy-related devices.

1. Introduction

Lithium-ion batteries (LIBs) are currently the main energy source of most portable electronic devices and electric vehicles worldwide.^[1] However, the flammable organic electrolytes in the LIBs have raised concerns over their safety especially in combination with Li-metal anodes for high-energy-density cells. To overcome this disadvantage of conventional LIBs, both academia and industry are dedicated to replacing liquid electrolytes with novel solid-state Li⁺ conductors that enable the use of metallic Li anodes.^[2] Among various solid-state Li⁺ conducting materials, the garnet solid electrolyte has drawn increasing

attention due to its high Li-ionic conductivity (up to 1 mS cm⁻¹ at 25 °C), broad electrochemical window (>6 V vs. Li⁺/Li) and intrinsic chemical stability toward metallic Li.^[3] However, even though garnets are in principle stable in air, they have been found to form a passivating surface layer in humid air that not only leads to challenges regarding the component fabrication and processing,^[4] but also hinders the Li⁺ conduction and thus impairs the battery performance.^[5] This instability of garnets against moisture is mainly attributed to the Li⁺/H⁺ exchange (LHX) reaction between garnets and water.^[6] Hence, understanding the mechanism of this LHX reaction can help with handling garnets in ambient atmosphere and solvents during processing and application. Understanding and ultimately mitigating the adverse effects of the LHX will be key to fully utilize the advantages of garnets, especially with respect to environmental friendliness of this fluorine-free, non-toxic electrolyte and the possibility for sustainable manufacturing of garnet-based batteries.


In this Minireview, we focus on the LHX in garnet solid electrolytes from fundamental to practical aspects. At the start, we provide a short introduction of garnet Li⁺ conductors. After showing the degradation phenomenon of garnets in humidity by LHX, we present the reaction mechanism behind the Li⁺/H⁺ chemistry and the impact of LHX on garnet structures and properties. The Minireview further introduces the up-to-date applications of LHX in solvent-assisted processing and garnets in water-based energy-related fields.

[a] R. Ye, Dr. M. Ihrig, Dr. M. Finsterbusch
Institute of Energy and Climate Research: Materials Synthesis and Processing (IEK-1)
Forschungszentrum Jülich GmbH
52425 Jülich (Germany)
E-mail: m.fensterbusch@fz-juelich.de

[b] R. Ye, Prof. E. Figgemeier
Institute for Power Electronics and Electrical Drives (ISEA)
RWTH Aachen University
52066 Aachen (Germany)
E-mail: e.figgemeier@fz-juelich.de

[c] Prof. N. Imanishi
Department of Chemistry for Materials, Graduate School of Engineering
Mie University
Tsu, Mie 514-8507 (Japan)

[d] Dr. M. Finsterbusch, Prof. E. Figgemeier
Helmholtz Institute Münster: Ionics in Energy Storage (HI-MS)
Forschungszentrum Jülich GmbH
48149 Münster (Germany)

 © 2021 The Authors. ChemSusChem published by Wiley-VCH GmbH. This is an open access article under the terms of the Creative Commons Attribution Non-Commercial NoDerivs License, which permits use and distribution in any medium, provided the original work is properly cited, the use is non-commercial and no modifications or adaptations are made.

2. Garnet Li⁺ Conductors

The first Li⁺ conductor of the garnet family was reported by Thangadurai et al. in 2003 as Li₅La₃Ta₂O₁₂ with a bulk conductivity around 10⁻⁶ S cm⁻¹ at 25 °C.^[7] Later, they showed an improved Li⁺ conductivity of 4 × 10⁻⁵ S cm⁻¹ at 22 °C for Li₆BaLa₂Ta₂O₁₂.^[8] In 2007, Murugan et al. achieved an important breakthrough with the Li-stuffed garnet Li₇La₃Zr₂O₁₂ (LLZO), which led to an enhancement in bulk conductivity by one order of magnitude to 3 × 10⁻⁴ S cm⁻¹ at 25 °C.^[9] Since then, the Li⁺ conductivity of LLZO was further increased to 10⁻³ S cm⁻¹ by introducing various dopants and substitutions like Al, Ta, Ga, and Nb.^[10]

Two stable crystal structures exist for LLZO: a cubic phase with the space group (SG) *Ia-3d* and a tetragonal phase with the space group *I4₁/acd*. The cubic LLZO has a Li⁺ conductivity two orders of magnitude higher than that of the tetragonal form.^[3a,d] Figure 1a shows the crystal structure of cubic LLZO that consists of 8-fold coordinated LaO₈ dodecahedra, 6-fold coordinated ZrO₆ octahedral, and Li ions partially occupying the interstitial sites. Based on neutron diffraction studies, the Li ions in cubic LLZO possess three different interstitial sites, namely (i) tetrahedral (24*d*), (ii) octahedral (48*g*), and (iii) off-centered octahedral (96*h*). As shown in Figure 1b, the 24*d* tetrahedral and the 48*g*/96*h* octahedral share the faces to each other, forming a Li⁺ pathway so that fast Li⁺ conduction is achieved in cubic LLZO. The 24*d* Li ions trapped in the tetrahedral site are immobile, whereas the Li ions on the 96*h* site, which are slightly off the 48*g* sites, are most anisotropic showing higher mobility.^[10a]

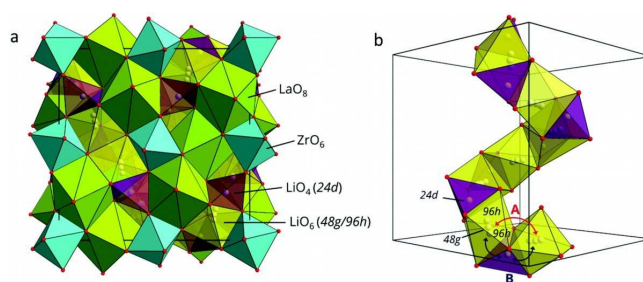
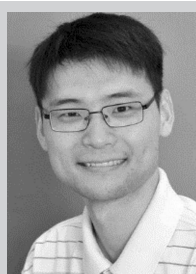


Figure 1. (a) Crystal structure of cubic Li₇La₃Zr₂O₁₂. (b) Wyckoff positions of Li ions and two potential Li⁺ migration pathways A (preferred in Li₅La₃M₂O₁₂) and B (preferred in Li₇La₃Zr₂O₁₂). Reprinted from Ref. [10a] with permission. Copyright 2019, Royal Society of Chemistry.

3. Li⁺/H⁺ Chemistry in Garnets

3.1. Instability of garnets against humidity

Although LLZO is in principle chemically stable in air so that the storage and processing of LLZO in ambient conditions is feasible, several studies reported the formation of a lithiophobic Li₂CO₃ layer on the LLZO pellet surface after exposure to air for a period of time, which is detrimental for the electrochemical performance of the material (e.g. large Li/garnet interfacial resistance due to the poor Li wettability of surface impurities).^[11] A widely accepted explanation for the degradation of LLZO in humidity is a two-step reaction route including the LHX LLZO and moisture in air [Eq. (1)] and the subsequent formation of Li₂CO₃ from the as-formed LiOH [Eq. (2)]:



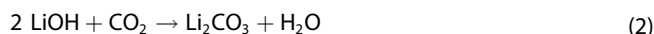
Ruijie Ye is doctoral researcher at Forschungszentrum Jülich (IEK-1) and RWTH Aachen University (ISEA) in Germany since he finished his chemistry study at Tongji University and Saarland University in 2018. His research interest lies in aqueous electrolytes and solid-state electrolytes (ceramic and polymer) for next-generation battery systems, and the water-based fabrication and processing thereof for the sake of sustainable battery production. In 2021 he was awarded a JSPS fellowship for a research stay in Prof. Imanishi's group at Mie University in Japan.



Martin Finsterbusch is head of the team "Solid State Batteries" at the Institute of Energy and Climate Research, Materials Synthesis and Processing (IEK-1), Forschungszentrum Jülich. After five years as research scientist at Montana State University, USA he received his PhD from Technische Universität Ilmenau in 2011. The same year, he started his Post-Doc at IEK-1 in the field of all-solid-state batteries. Since 2016 he develops with his team ceramic-based components and cells for next-generation Li and Na batteries as well as ion beam-based analysis techniques for operando battery analysis.



Egbert Figgemeier obtained his Ph.D. in physical chemistry from University of Paderborn. This was followed by academic research at the Universities of Dublin, Basel, and Uppsala. In 2007, he joined Bayer Technology Services to head the materials and corrosion laboratory, as well as to develop materials for battery applications. From 2012, he worked as Application Development Engineer for battery materials at 3 M Deutschland and was responsible for technical supports of customers in Germany and Europe. Since 2016, he has been a group leader at the Helmholtz Institute Münster (section Aachen) and he holds the chair for Ageing and Reliability of Batteries at RWTH Aachen University.



Besides, the $\text{LiOH}\cdot\text{H}_2\text{O}$ formed from the LiOH can be a necessary intermediate prior to or simultaneously with the reaction with CO_2 to form Li_2CO_3 .^[12]

Since the LHX is the key step in the degradation of LLZO in humidity, many investigations regarding LHX were carried out on various garnets [i.e., $\text{Li}_5\text{La}_3\text{M}_2\text{O}_{12}$ ($\text{M}=\text{Ta}$, Nb),^[13] $\text{Li}_6\text{MLa}_2\text{Nb}_2\text{O}_{12}$ ($\text{M}=\text{Ca}$, Ba)^[14] and $\text{Li}_7\text{La}_3\text{Zr}_2\text{O}_{12}$ with different substitutions (e.g. Al , Ta , Nb)^[15]] in aqueous solutions or organic acids. In most cases, severe Li losses in garnets along with a pH increase of the aqueous solutions were observed, indicating the LHX according to Equation (1).

3.2. Mechanism

So far, the general LHX mechanism for garnets is not yet clarified due to the complications introduced by the replacement of Li ions with protons, which is highly dependent on the garnet composition and substitution content.

Ma et al. proposed a LHX mechanism for polycrystalline cubic $\text{Li}_7\text{La}_3\text{Zr}_2\text{O}_{12}$ powder in water at room temperature.^[15e] The LHX preferentially occurs at the most anisotropic Li site, 96 *h*, leaving both 48 *g* and 24*d* sites largely unaffected. With the depletion of Li^+ on the 96 *h* site, the 48 *g* site might be further dominant in the exchange, but no LHX takes place at the 24*d* site. As a result, the final product of the water treatment has its 24*d* sites occupied by Li ions, 48 *g* sites occupied by Li ions and protons, and 96 *h* sites solely occupied by protons. This is consistent with the observation by Li et al. on $\text{Li}_{6.5}\text{La}_3\text{Zr}_{1.5}\text{Ta}_{0.5}\text{O}_{12}$ that the Li-ion occupancy of the 24*d* sites is the same before and after LHX, whereas those of 48 *g* and 96 *h* sites are reduced after LHX.^[16] Liu et al.^[15c] and Hiebl et al.^[17] supported this explanation, based on the investigation on $\text{Li}_{6.75}\text{La}_3\text{Nb}_{0.25}\text{Zr}_{1.75}\text{O}_{12}$ and single-crystal Al-substituted LLZO, respectively. It has also been found that the crystal structure of LLZO maintains centric *la-3d* during the LHX process but with a minor lattice expansion due to the replacement of strong Li–O bonds with the weaker O–H...O bonds.^[15e,18] Modelling suggests this lattice expansion has a linear correlation versus the retained Li content in LLZO.^[19]

In contrast, Truong and Thangadurai found that Li ions at the tetrahedral sites in $\text{Li}_{5+x}\text{Ba}_x\text{La}_{3-x}\text{Nb}_2\text{O}_{12}$ favor the LHX while octahedral-site ions are rather stable.^[20] Similarly, Nyman et al. suggested that Li ions in the tightly bound, immobile sites in $\text{Li}_5\text{La}_3\text{Ta}_2\text{O}_{12}$ are removed by LHX with protons.^[13a] Recently, Redhammer et al. also found that LHX occurs preferably at the 24*d* sites in single-crystal $\text{Li}_6\text{La}_3\text{ZrTaO}_{12}$.^[21] It could be attributed to the small displacement of Li^+ away from 24*d* to a general 96 *h* position due to the Ta-substitution, which leads to an enhanced mobility of Li^+ at 24*d* sites. This displacement does not alter the garnet *la-3d* structure at 27 °C. In the case of the

LHX taking place at 90 °C, a symmetry reduction from *la-3d* to non-centrosymmetric *I-43d* is observed, and the preferable LHX occurs at the 48e site (equivalent to the 96 *h* site). However, Liu et al. addressed that this phase transition can take place even at room temperature for $\text{Li}_{6.25}\text{Al}_{0.25}\text{La}_3\text{Zr}_2\text{O}_{12}$ with an intensive exchange (> 75 %).^[22] Galven et al. reported a similar observation when $\text{Li}_6\text{CaLa}_2\text{Nb}_2\text{O}_{12}$ was treated in refluxed acetic acid.^[14a] In addition, there have been another two symmetries reported for protonated $\text{Li}_5\text{La}_3\text{Nb}_2\text{O}_{12}$, namely the non-centric cubic *I2,3* and the orthorhombic *P2,2,2*.^[13b,23] These symmetry changes as well as the structural disorders are generally induced by the change of site occupation and atomic interaction between Li, H, and O ions.

3.3. Phase transition from tetragonal to cubic

The phase transition from tetragonal to cubic induced by LHX has been firstly observed by Galven et al. for the tetragonal $\text{Li}_7\text{La}_3\text{Sn}_2\text{O}_{12}$ with SG *I4,acd*, which turned into cubic $\text{Li}_{2.25}\text{H}_{4.75}\text{La}_3\text{Sn}_2\text{O}_{12}$ with SG *la-3d* after a treatment in refluxed benzoic acid/ethanol solution.^[15d] The correspondence between the Li^+ sites in the two structures was described as following (Figure 2a): i) the 24*d* site in the cubic phase are derived from 8*a* (fully occupied by Li^+) and 16*e* (vacancies) sites of the tetragonal one; ii) the 48 *g* site of cubic phase originates from 32 *g* and 16*f* (both occupied by Li^+) in the tetragonal phase; iii) the 96 *h* sites in cubic phase are the former empty 32 *g* sites in the tetragonal one. Later, the same phase transition in LLZO triggered by humidity in air was observed as well. According to Larraz et al., the phase transition caused by protonation is irreversible upon heating above 650 °C,^[24] while the cubic phase without LHX is formed solely by reaching the tetragonal→cubic phase-transition temperature for LLZO (625–645 °C) and returns to tetragonal phase after cooling (Figure 2b).^[25] Moreover, Orera et al. claimed that a non-centrosymmetric *I-43d* cubic phase is obtained below 150 °C after the protonation of tetragonal LLZO,

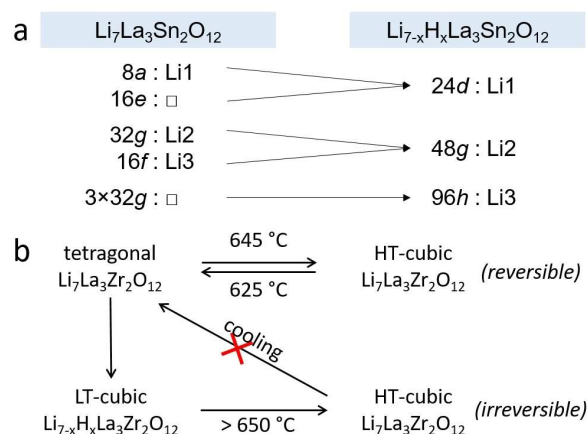


Figure 2. (a) Correspondence between the Li sites in the two garnet structures: tetragonal $\text{Li}_7\text{La}_3\text{Sn}_2\text{O}_{12}$ and cubic $\text{Li}_{7-x}\text{H}_x\text{La}_3\text{Sn}_2\text{O}_{12}$. Reproduced from Ref. [15d] with permission. Copyright 2011, American Chemical Society. (b) Phase transition between tetragonal, LT-, and HT-cubic $\text{Li}_7\text{La}_3\text{Zr}_2\text{O}_{12}$.

while annealing above 300 °C results in a centric *la-3d* cubic phase with lower H⁺ content.^[15f] Overall, these findings suggest that H⁺ can act as a dopant to stabilize the cubic structure of LLZO. This cubic garnet structure stabilized by H⁺ is usually called low-temperature (LT) cubic garnet structure.^[26] In contrast, the cubic phase without LHX is called high-temperature (HT) cubic garnet.

3.4. Kinetics

Figure 3 a presents the tendency of Li loss in garnets upon the duration of LHX in water or acids based on 13 references as listed in Table S1. It is a challenge selecting the most water-stable garnets, because the Li losses of the garnets even with the same composition vary among different reports. This might be attributed to different test conditions and characterization methods. However, it is revealed from Figure 3a that powders, due to larger surface area, usually show higher LHX than pellets. Depth profile analyses of garnet samples exposure to humid air

revealed that Li₂CO₃ and LiOH with a gradient distribution were only detected in the first 400 nm of the samples (Figure 3b).^[11b,27] The LHX is usually assumed to be fast in the very beginning at the surface of garnets towards water, which leads to an H⁺-enriched garnet surface layer. This surface layer consequently hinders the further reaction of water with the interior positions in the garnet and can thus be considered somewhat self-limiting. A study on LHX behavior of polycrystalline Li₆La₃ZrTaO₁₂ powder in different surroundings (Figure 3c) revealed that the exchange rates in all conditions are similar (0.9–1.8 × 10⁻¹⁹ mol s⁻¹) except for the one in warm water (4.6 × 10⁻¹⁹ mol s⁻¹), which results in a much higher estimated H⁺ equilibrium concentration than others. Hence, it is believed that the reaction kinetics is more limited by the temperature-dependent proton diffusion inside garnets rather than by the H⁺ concentration in aqueous/acid media.^[21] Hiebl et al. determined the H⁺ diffusion coefficient as 2 × 10⁻¹⁷ m²s⁻¹ in a protonated Al-doped LLZO.^[17]

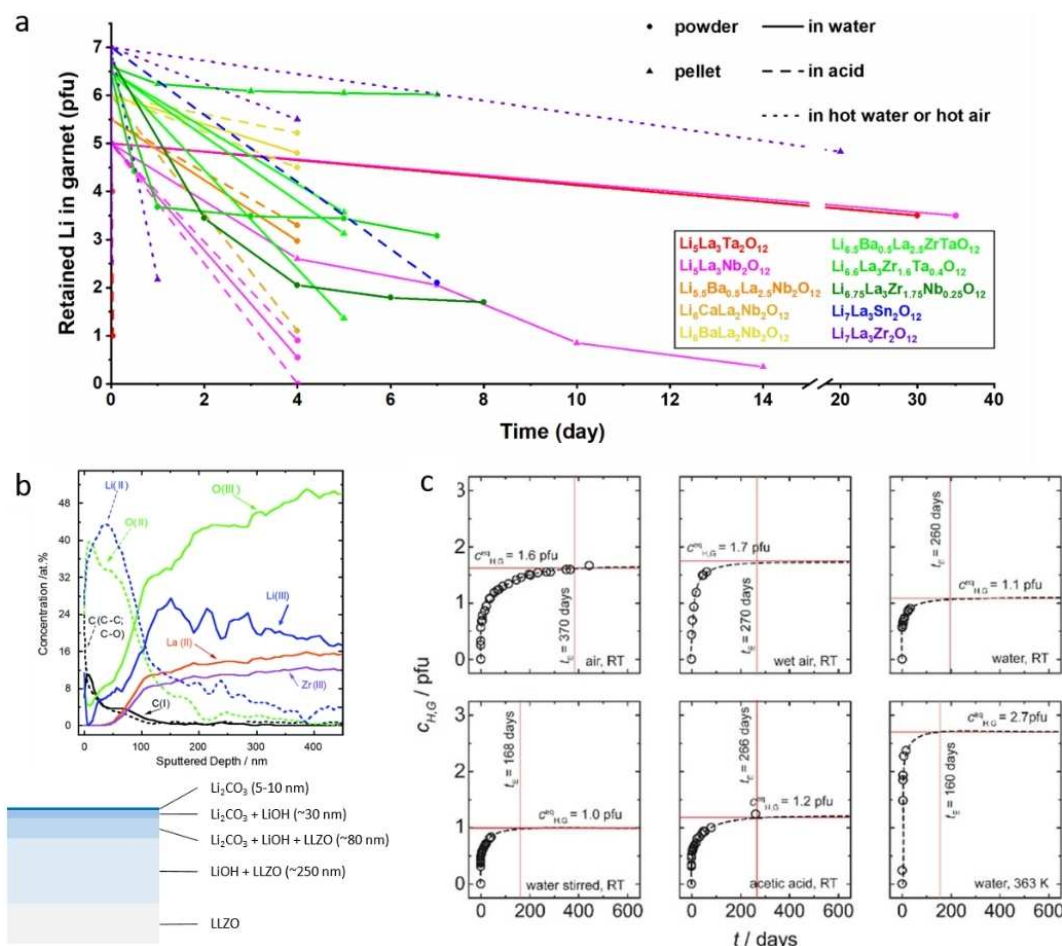


Figure 3. (a) Retained Li content in garnet after aqueous or acid treatments based on references listed in Table S1. (b) Depth profile for the concentration of Li, C, O, Zr, and La from the X-ray photoelectron spectroscopy analysis of garnet after preparation in ambient air and a corresponding schematic depicting the contamination layers. Reproduced from Ref. [11b] with permission. Copyright 2017, Royal Society of Chemistry. (c) Concentration profiles for garnet powder, fitted exponentially to estimate qualitatively the H⁺ equilibrium concentration $c_{H,G}^{(eq)}$. Reprinted from Ref. [21] with permission. Copyright 2020, American Chemical Society.

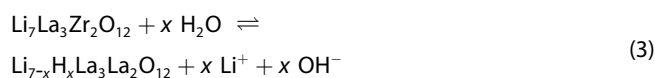
Table 1. Investigations on reverse Li⁺/H⁺ exchange of garnets.

Entry	Protonated garnets	Condition ^[a]	Composition after reverse LHX	Ref.
1	Li _{0.56} H _{4.44} La ₃ Nb ₂ O ₁₂	5 M LiNO ₃ , RT, 4 days	"Li ₅ La ₃ Nb ₂ O ₁₂ "	[20]
2	Li ₃ H _{2.5} Ba _{0.5} La _{2.5} Nb ₂ O ₁₂	5 M LiNO ₃ , RT, 4 days	"Li _{5.5} Ba _{0.5} La _{2.5} Nb ₂ O ₁₂ "	[20]
3	Li _{4.8} H _{1.2} BaLa ₂ Nb ₂ O ₁₂	5 M LiNO ₃ , RT, 4 days	"Li ₆ BaLa ₂ Nb ₂ O ₁₂ "	[20]
4	Li _{1.70} H _{5.05} La ₃ Zr _{1.75} Nb _{0.25} O ₁₂	5 M LiNO ₃ , 25 °C, 4 days	Li _{1.73} H _{5.02} La ₃ Zr _{1.75} Nb _{0.25} O ₁₂	[15c]
5	Li _{1.70} H _{5.05} La ₃ Zr _{1.75} Nb _{0.25} O ₁₂	5 M LiNO ₃ , 60 °C, 24 h	Li _{1.90} H _{4.85} La ₃ Zr _{1.75} Nb _{0.25} O ₁₂	[15c]
6	Li _{1.70} H _{5.05} La ₃ Zr _{1.75} Nb _{0.25} O ₁₂	5 M LiNO ₃ , 60 °C (ht), 24 h	Li _{1.91} H _{4.84} La ₃ Zr _{1.75} Nb _{0.25} O ₁₂	[15c]
7	Li _{1.70} H _{5.05} La ₃ Zr _{1.75} Nb _{0.25} O ₁₂	sat. LiOH, 60 °C (ht), 24 h	Li _{2.98} H _{3.77} La ₃ Zr _{1.75} Nb _{0.25} O ₁₂	[15c]
8	Li _{2.55} H _{4.45} La ₃ Zr ₂ O ₁₂	2 M LiOH, RT, 15 min	Li _{4.15} H _{2.85} La ₃ Zr ₂ O ₁₂	[15e]
9	Li _{3.08} H _{3.52} La ₃ Zr ₂ Ta _{0.4} O ₁₂	1 M LiOH, RT	Li _{5.36} H _{1.24} La ₃ Zr ₂ Ta _{0.4} O ₁₂	[15b]
10	Li _{3.44} H _{3.16} La ₃ Zr ₂ Ta _{0.4} O ₁₂	1 M LiOH, RT	Li _{5.54} H _{1.06} La ₃ Zr ₂ Ta _{0.4} O ₁₂	[15b]
11	Li _{3.49} H _{3.11} La ₃ Zr ₂ Ta _{0.4} O ₁₂	1 M LiOH, RT	Li _{5.64} H _{0.96} La ₃ Zr ₂ Ta _{0.4} O ₁₂	[15b]
12	Li _{3.68} H _{2.92} La ₃ Zr ₂ Ta _{0.4} O ₁₂	1 M LiOH, RT	Li _{6.04} H _{0.56} La ₃ Zr ₂ Ta _{0.4} O ₁₂	[15b]
13	Li _{6.53} H _{0.07} La ₃ Zr ₂ Ta _{0.4} O ₁₂	1 M LiOH, RT	Li _{6.53} H _{0.07} La ₃ Zr ₂ Ta _{0.4} O ₁₂	[15b]
14	Li _{6.86} H _{0.14} La ₃ Zr ₂ O ₁₂	surface Li ₂ CO ₃ , 700 °C, 15 min	Li ₇ La ₃ Zr ₂ O ₁₂	[24]
15	Li _{5.4} H _{1.6} La ₃ Zr _{1.4} Nb _{0.6} O ₁₂	LiNO ₃ + LiOH powder, 400 °C, 98 MPa, 6 h	Li _{6.4} La ₃ Zr _{1.4} Nb _{0.6} O ₁₂	[28]

[a] RT: room temperature; sat.: saturated; ht: hydrothermal.

3.5. Reversibility

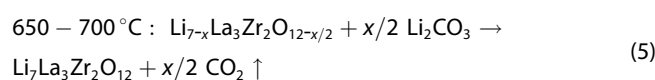
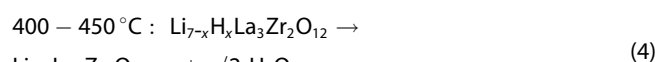
Several reports, as summarized in Table 1, have shown the phenomenon of reverse LHX in garnets, that is, Li⁺ reenter the protonated garnets to replace H⁺. If the chemical formula [Eq. (1)] is written in ionized chemical balance, we obtain Equation (3):



In order to shift the equilibrium to the left side, we can, according to the principle of Le Chatelier, either remove water from the system or increase the concentration of Li⁺ and/or OH⁻, for example, by adding Li salts and/or alkali.

Concentrated Li salt and/or base aqueous solutions [e.g., LiCl and LiOH solutions (>1 M)] have been proven to sufficiently suppress the occurrence of LHX for pristine garnets (e.g., entry 13 in Table 1).^[13d,14b,15b,29] The high chemical potential of Li⁺ and/or OH⁻ in the aqueous media pushes the chemical balance [Eq. (3)] towards the left side, meaning that the LHX is hardly happening. However, to our knowledge, a complete reverse exchange of already protonated garnets has not been achieved in aqueous solutions yet. This might be related to the energy barrier of the replacement of H⁺ by Li⁺. The closest attempt to completion was performed by Truong and Thangadurai (entry 1 in Table 1).^[20] The reverse-ion-exchanged Li₅La₃Nb₂O₁₂ has a cell constant of $a = 12.789(3) \text{ \AA}$, which is only slightly larger than the pristine one [12.775(2) Å], and no significant weight loss (only ≈ 0.5%) between 300 and 500 °C was observed, indicating only limited decomposition due to H-substitution.

On the other hand, a complete reverse LHX can be accomplished by thermal treatment with the presence of additional Li sources.^[30] Larraz et al. proposed this thermal evolution of LLZO from its protonated form as following steps [Eqs. (4) and (5)]:^[24]



With the help of an in-situ synchrotron-based high-energy X-ray diffraction technique (HEXRD) (Figure 4) Cai et al. recently suggested that the stoichiometric restoration of LLZO can be completed at higher temperatures (730–950 °C) due to the increased melting point of the eutectic solution of LiOH and Li₂CO₃, thereby impeding the reverse LHX.^[31] In this process the stoichiometric LLZO is formed via the reaction of Li₂CO₃ with the intermediate La₂Zr₂O₇, which is the decomposition product of protonated LLZO by heating.

Alternatively, a combination of LiNO₃ and LiOH enables the Li recovery at lower temperature due to their lower melting

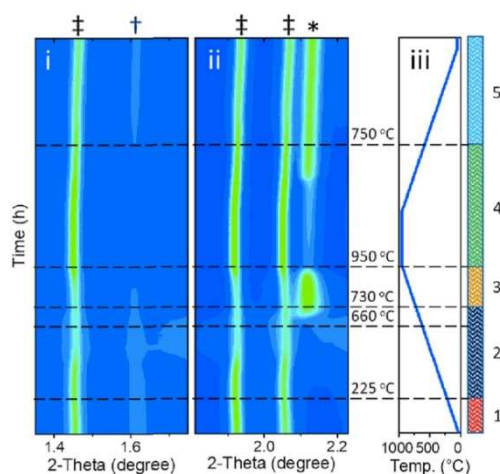
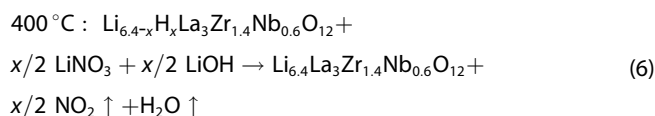


Figure 4. High-temperature in-situ HEXRD phase evolutions of LLZO. The "‡", "‡*", and "†" symbols stand for LLZO, La₂Zr₂O₇, and Li₂CO₃, respectively. Reprinted from Ref. [31] with permission. Copyright 2021, Elsevier.

points than Li_2CO_3 , resulting in the overall reaction shown in Equation (6):^[28]



3.6. Ion mobility and conductivity

Sanjuán et al. proposed a concerted Li^+ – H^+ diffusion mechanism in $\text{Li}_{5-x}\text{H}_x\text{La}_3\text{Nb}_2\text{O}_{12}$ (Figure 5a).^[23] Li^+ hopping from a tetrahedral to an octahedral site can only occur if there is no H^+ inside the target cage and vice versa. For instance, the Li^+ move #1 is allowed but the move #1' is not. Similarly, the H^+ move #4 is restricted if the tetrahedral site is occupied by Li^+ . In addition, H^+ reorientation around a tetrahedral (#2) liberates an octahedral vacancy which may be occupied by the neighboring Li^+ (#5). Therefore, the Li^+ migration must be along with the H^+ movement simultaneously. Besides, the stable O–H bonding is expected to prevent H^+ mobility, leading to a lower Li^+ mobility in the protonated garnet than in non-exchanged

form.^[15] Liu et al. recently differentiated the conduction behavior of H^+ and Li^+ ions in $\text{Li}_{6.25-x}\text{H}_x\text{Al}_{0.25}\text{La}_3\text{Zr}_2\text{O}_{12}$ at various temperature (Figure 5b) and claimed that H^+ ions are immobile at room temperature and have enhanced mobility only at elevated temperatures, while the Li^+ ions always maintain a good mobility over the whole temperature range.^[22] However, the Li^+ conductivity is expected to be reduced by two orders of magnitude upon a high degree of LHX, which is consistent with the results of molecular dynamics simulation made by Yow et al. (Figure 5c).^[15b] The Li^+ mobility with an activation energy of 0.32 eV is hardly affected and clearly dominates over the H^+ mobility in the $\text{Li}_{6.5}\text{H}_{0.5}\text{La}_3\text{Zr}_2\text{O}_{12}$ that shows only minor proton exchange. In the case of high degree of LHX (i.e., $\text{Li}_3\text{H}_4\text{La}_3\text{Zr}_2\text{O}_{12}$ in Figure 5c) the activation energy for Li^+ migration is increased to 0.85 eV, while the H^+ maintains a lower energy barrier of 0.58 eV for its migration. Thus, $\text{Li}_3\text{H}_4\text{La}_3\text{Zr}_2\text{O}_{12}$ shows a mixed H^+ and Li^+ conductivity.

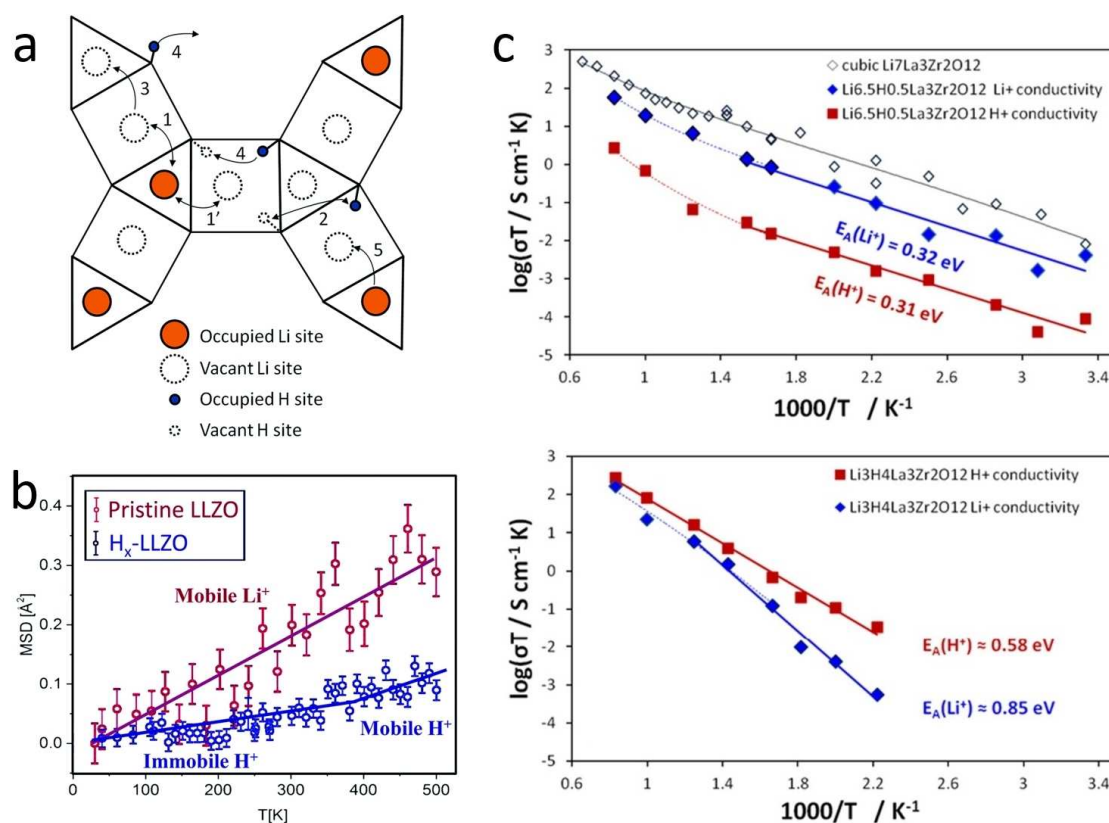


Figure 5. (a) Scheme depicting possible Li^+ and H^+ exchange events depending on occupancy of available sites. The tetrahedral is represented by triangle and octahedral by square. Reprinted from Ref. [23] with permission. Copyright 2018, Royal Society of Chemistry. (b) Average mean-square-displacement (MSD) of pristine and protonated garnets. Reprinted from Ref. [22] with permission. Copyright 2019, Royal Society of Chemistry. (c) Arrhenius plots of Li^+ and H^+ ionic conductivity derived from the MSD of the respective mobile species in molecular dynamics simulations of the protonated LLZO. Reprinted from Ref. [15b] with permission. Copyright 2016, Elsevier.

4. Sustainable Applications

4.1. Solvent-assisted processing

The LHX of garnets was also observed in several common organic solvents, which was shown by the change of the lattice parameter in $\text{Li}_{6.25}\text{Al}_{0.25}\text{La}_3\text{Zr}_2\text{O}_{12}$ after immersion (Figure 6).^[19] Especially, primary alcohols such as ethanol, methanol, and 1-propanol have significant LHX rates due to the higher acidity and reactivity of the hydroxyl group [Eq. (7)]:



2-Propanol is a special case, where less LHX occurred due to the weaker acidic character of the secondary alcohol as well as a possible steric hindrance. In comparison, aprotic solvents without proton-giving functional groups such as cyclohexane and acetonitrile react much less with garnets. Therefore, aprotic solvents are recommended for wet processing of garnets to prevent LHX. Another study on solvent-assisted ball-milling showed that acetonitrile successfully limits the Li loss of $\text{Li}_{6.4}\text{La}_3\text{Zr}_{1.4}\text{Ta}_{0.6}\text{O}_{12}$ to a mere 4%, whereas the powder milled in ethanol showed a Li loss of approximately 30%.^[32]

However, in large-scale powder production, organic solvents usually cause safety, cost, and recycling issues. Hence, water-based processing is highly attractive to facilitate a more sustainable “green” industrial-scale production.^[33] Nevertheless, the final component properties of water-processed LLZO need to match the ones from the organic route in order to maintain the attractive electrochemical performance of LLZO. To that regard, Truong and Thangadurai found that the reverse-ion-exchanged $\text{Li}_5\text{La}_3\text{Nb}_2\text{O}_{12}$ (entry 1 in Table 1) had better sinterability than the pristine one and thus higher Li-ionic conductivity.^[20] Huang et al. demonstrated an aqueous powder processing route for $\text{Li}_{6.4}\text{La}_3\text{Zr}_{1.4}\text{Ta}_{0.6}\text{O}_{12}$ combining the water-based attrition milling with the spray drying (Figure 7a).^[34]

Uniform fine garnet powder with a particle size of 300 nm was prepared by attrition milling and formed large sphere-like secondary granulates of 5–20 μm after subsequent spray drying. The pellets sintered from this powder had a relative density close to 94% and a conductivity of 0.419 mS cm^{-1} at room temperature. Peng et al. introduced an aqueous-based gel-casting process to fabricate $\text{Li}_{6.4}\text{La}_3\text{Zr}_{1.4}\text{Ta}_{0.6}\text{O}_{12}$ solid electrolytes (Figure 7b), which had a high Li-ionic conductivity of 0.74 mS cm^{-1} at 25°C .^[35] This gel-casting technique proved suitable to fabricate structured garnet electrolytes by casting on elaborate molds. Moreover, sustainable fabrication of thin freestanding $\text{Li}_{6.45}\text{Al}_{0.05}\text{La}_3\text{Zr}_{1.6}\text{Ta}_{0.4}\text{O}_{12}$ separators were recently presented by us via a water-based tape-casting process (Figure 7c).^[15a] The thickness of the dense garnet separators produced via this “green” manufacturing route can be reduced below $150 \mu\text{m}$, which is much smaller than the conventionally sliced garnet pellets with thicknesses above $300 \mu\text{m}$, and can thus further decrease the inner resistance of a solid-state Li battery. In addition, Jonson et al. reported recently that 5 wt% MgO can help densify the water-based tapes and enhance the ionic conductivity.^[36] When the tape-cast aqueous slurry is freeze-dried, vertically oriented porous structures can be obtained in the garnet layers (Figure 7d).^[37] The garnet frameworks fabricated by this freeze-casting technique can be applied as structural support for composite cathodes that have improved Li-ionic conduction compared to electrodes from pure cathode active material or highly tortuous composite cathodes from powder mixing.

The LHX can be reversed at elevated temperature in the presence of excess Li sources (see Section 3.5), for which LiOH and Li_2CO_3 are commonly used in these above-mentioned water-based methods. Therefore, aqueous processing of garnets is harmless to the electrochemical performance, if a final sintering step at temperatures around 1000°C is used. Thus, suitable routes for a sustainable fabrication of garnet-based battery components exist, but challenges remain regarding

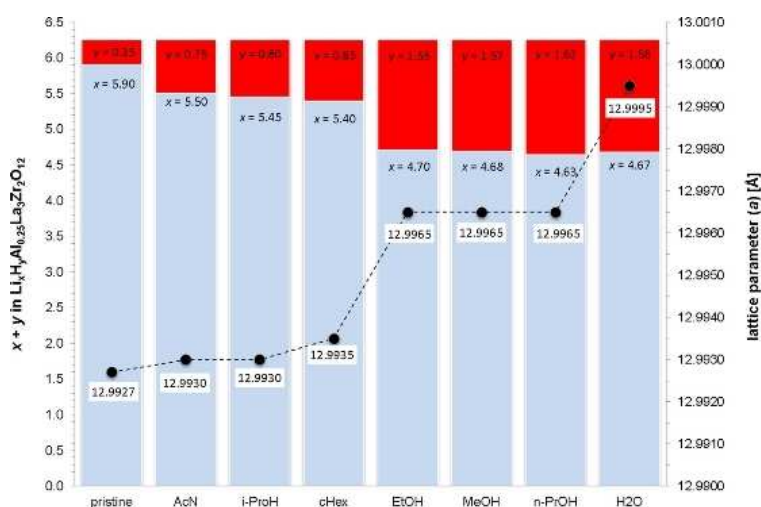


Figure 6. Residual Li stoichiometry and lattice parameter of garnet $\text{Li}_{6.25}\text{Al}_{0.25}\text{La}_3\text{Zr}_2\text{O}_{12}$ powder after immersion in solvents. Reprinted from Ref. [19] with permission. Copyright 2018, American Chemical Society.

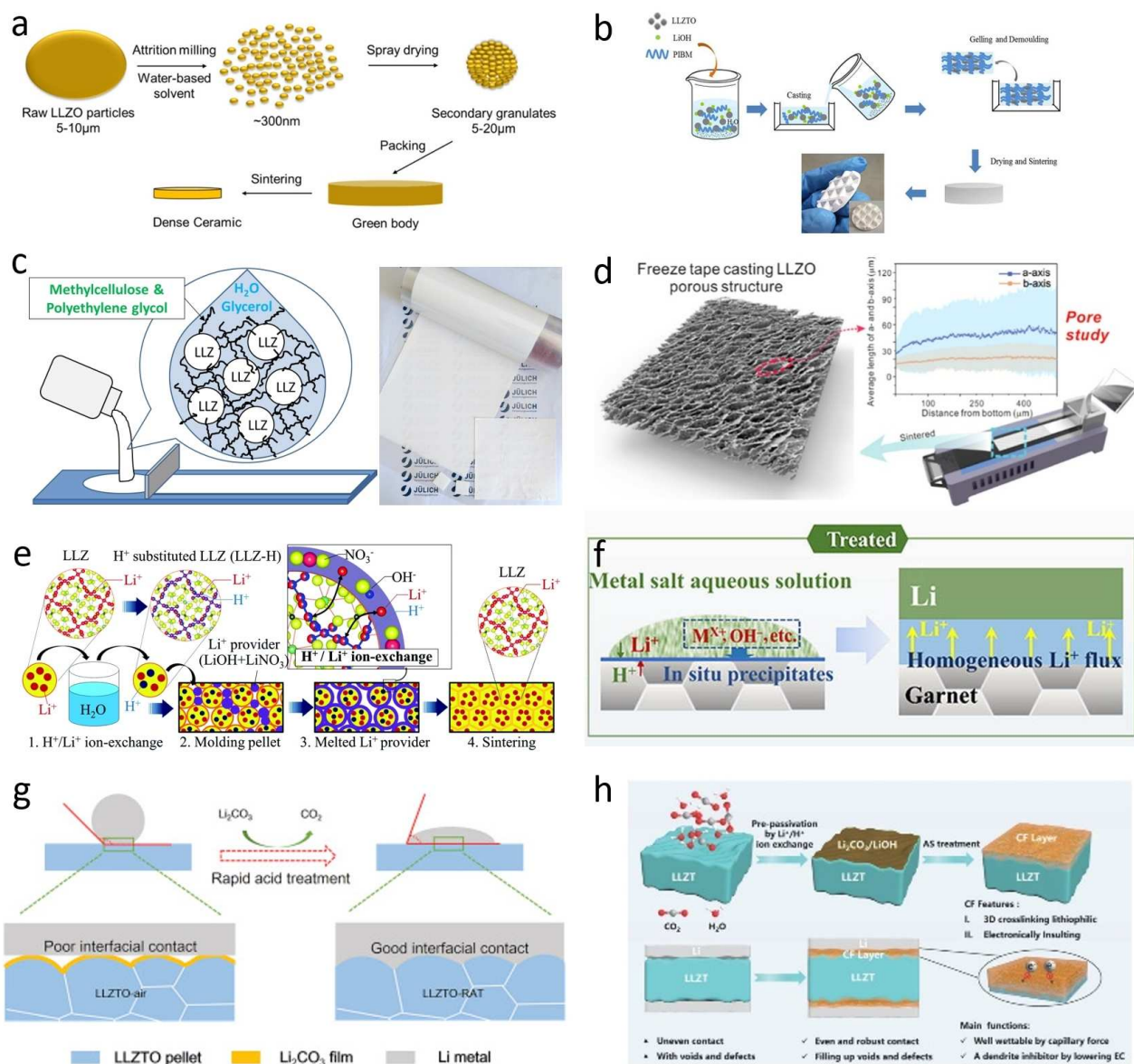


Figure 7. Water-based processing of garnets. (a) Attrition-milling and spray-drying. Reprinted from Ref. [34] with permission. Copyright 2018, American Chemical Society. (b) Gel-casting. Reprinted from Ref. [35] with permission. Copyright 2019, Wiley. (c) Tape-casting. Reprinted from Ref. [15a] with permission. Copyright 2020, Royal Society of Chemistry. (d) Freeze-casting. Reprinted from Ref. [37c] with permission. Copyright 2019, American Chemical Society. (e) Hot-pressing. Reprinted from Ref. [28] with permission. Copyright 2020, Royal Society of Chemistry. (f) In-situ metal oxide formation. Reprinted from Ref. [40b] with permission. Copyright 2019, Elsevier. (g) Rapid acid treatment for interfacial engineering. Reprinted from Ref. [41] with permission. Copyright 2019, Elsevier. (h) LiF-LiCl modification of garnet surface. Reprinted from Ref. [43] with permission. Copyright 2021, Wiley.

low-temperature sintering, which is often necessary to incorporate high-energy-density cathode active materials.^[38]

Wang et al. densified Li_{6.1}Al_{0.3}La₃Zr₂O₁₂ by cold sintering at 350 °C using water or HNO₃ as aqueous media.^[39] Although relative densities around 90% were achieved, the Li-ion conductivities of the cold-sintered garnet pellets were found to be five orders of magnitude lower than the ones obtained by conventional sintering. This degradation of conductivity was likely due to the dissolution of Al species from the Al-substituted garnet and its precipitation on the grain boundaries, which severely hinders the Li⁺ conduction among grains.

Ohta et al. achieved the sintering of Li_{6.4}La₃Zr_{1.4}Nb_{0.6}O₁₂ triggered by a reverse LHX reaction at 400 °C, which further enabled the densification of composite cathode consisting of this garnet and LiNi_{1/3}Co_{1/3}Mn_{1/3}O₂.^[28] As shown in Figure 7e, LiOH and LiNO₃ play the role as Li⁺ providers to recover the Li content in protonated garnet during the hot pressing. It is notable that a high pressure (98 MPa in this research) is necessary in this process to assist densification. The sintered garnet pellet had 90% relative density and a Li⁺ conductivity of 0.22 mS cm⁻¹ at 25 °C. Moreover, the solid-state Li battery prepared by the same method shows a low interfacial resistance

around $200 \Omega \text{ cm}^2$ (both cathode and anode sides), which is promising for industrial battery application.

LHX can also be involved in constructing a tailored Li/garnet interface. Cai et al. demonstrated such aqueous strategy for in-situ lithiophilic metal oxide (e.g., Ag_2O , ZnO , PbO) layer formation (Figure 7f).^[40] After dropping an aqueous metal salt precursor solution onto garnet surface, it reacted with the LiOH released by LHX of garnet to form a deposition layer, which is further decomposed to corresponding metal oxide by a rapid heat treatment. These metal oxide layers serve as mixed Li-ionic and electronic conductive interlayers, which lead to uniform Li ion flow and a significant reduction of Li/garnet interfacial resistance to around $10 \Omega \text{ cm}^2$ at room temperature.

The passivation layers on the surface of air-aged garnets consisting of the LHX products Li_2CO_3 and LiOH are conventionally removed by thermal decomposition at $500\text{--}750^\circ\text{C}$.^[4a,11a] However, this processing step is energy- and time-consuming. Recently, rapid acid treatments have been developed for removing and retrieving the lithiophilic surface of garnets (Figure 7g). Huo et al. applied 1 M HCl aqueous solution to transform the lithiophobic Li_2CO_3 into a lithiophilic LiCl layer.^[41] Similarly, H_3PO_4 and NH_4F have also been used to form a Li_3PO_4 and LiF coating, respectively.^[42] As shown in Figure 7h, Ruan et al. employed mixed aqueous acids of HCl and HF to build a 3D cross-linking LiCl-LiF surface, which is not only lithiophilic but also electronically insulating, leading to effective suppression of Li dendrite penetration.^[43] It is notable that the acid treatment time should be controlled precisely because excess acid could corrode the bulk garnet and thus lower its Li-ionic conductivity.

4.2. Aqueous lithium metal batteries and relatives

Aqueous lithium metal batteries (ALBs) combine the advantages of Li metal anodes [i.e., the low redox potential (-3.04 V vs. standard hydrogen electrode) and high theoretical capacity (3869 mAh g^{-1})] with the advantages of aqueous electrolytes (i.e., the high Li-ionic conductivity and safety as well as environmental friendliness).^[44] Hence, they are promising candidates for sustainable high-density energy storage. However, metallic Li is unstable in direct contact with aqueous electrolytes. One approach to protect the metallic Li anodes from aqueous electrolytes is to introduce a dense ceramic solid electrolyte separator (Figure 8a). Most garnets show intrinsic chemical stability toward Li metal, and several of them are also highly stable in concentrated Li salt/base aqueous solutions. Their high density ensures the protection of the metallic Li from water. In addition, garnets can provide high Li^+ conduction and eliminate H^+ crossover.^[22] Imanishi et al. evaluated the possible application of garnet separator in aqueous Li-air batteries, and found that the garnet separators suffered from fast short circuit due to Li dendrite growth at high current (e.g., 0.5 mA cm^{-2}), though the garnet had a relatively high density and was supposed to suppress the Li dendrite formation.^[29a,b,45] Thus, an interfacial modification of garnet separators on the anode side is needed to eliminate this limiting factor for the application of garnets in ALBs. Liu and Wang demonstrated a Li- H_2O_2 semi-fuel cell,^[46] in which a garnet $\text{Li}_{6.4}\text{La}_3\text{Zr}_{1.4}\text{Ta}_{0.6}\text{O}_{12}$ thin sheet ($200 \mu\text{m}$ thick, $\approx 94\%$ relative density) was applied to separate the organic electrolyte [1 M LiPF_6 in ethylene carbonate and diethyl carbonate (1:1 v/v)] on anode side and the flowing aqueous electrolyte (2 M LiCl and 0.1 M H_2O_2 in H_2O) on the

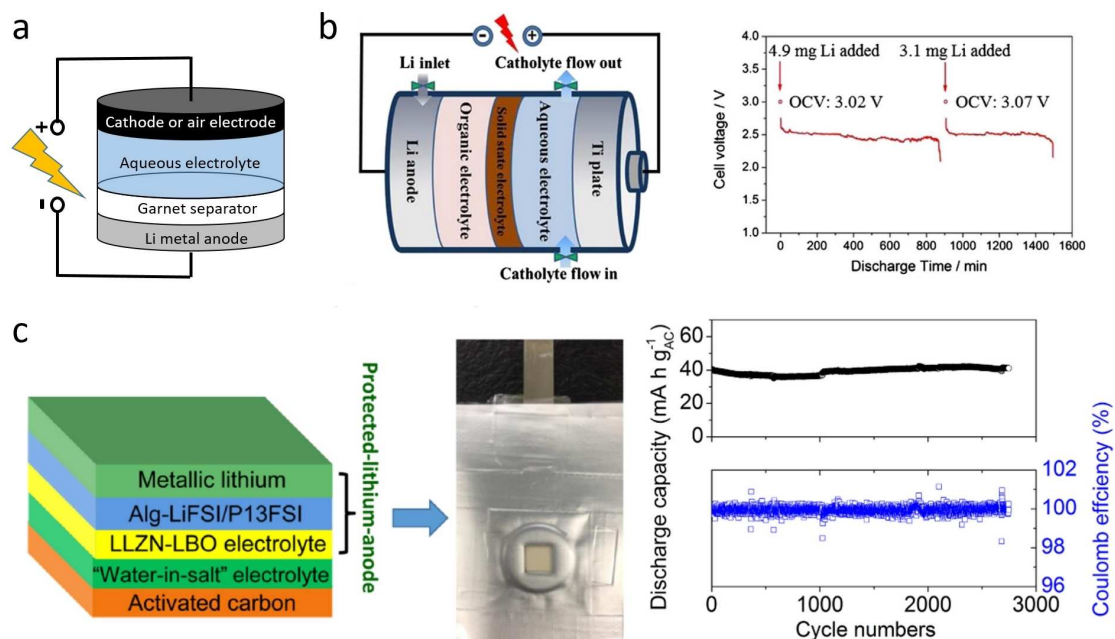


Figure 8. (a) Schematic of structure of an aqueous lithium metal battery. (b) Li- H_2O_2 semi-fuel cell. Reprinted from Ref. [46] with permission. Copyright 2014, Elsevier. (c) Aqueous Li ion capacitor. Reprinted from Ref. [47] with permission. Copyright 2020, Elsevier.

cathode side (Figure 8b). This semi-fuel cell gave a stable discharge at 2.5 V for 1500 min with a constant current of 0.44 mA cm⁻², and the average utilization of Li metal in the anode was 82%. Recently, Zhan et al. demonstrated an aqueous Li ion capacitor equipped with the garnet Li_{6.75}La₃Zr_{1.75}Nb_{0.25}O₁₂ as protection layer for metallic Li.^[47] Concentrated LiTFSI aqueous solution was used as electrolyte on the cathode side, whereas a gel polymer was applied on the other side to improve the interface between garnet and Li metal anode (Figure 8c). This capacitor delivered a capacity of 30.1 mAh g⁻¹, a specific energy of 78.7 Wh kg⁻¹ and a specific power of 6.6 kW kg⁻¹ with 0.5 mA cm⁻² at 60 °C.

5. Summary and Outlook

Li⁺/H⁺ exchange (LHX) unavoidably occurs when Li garnets are exposed to ambient air containing moisture, as well as in aqueous and acidic solution and primary alcohols. The initially very fast reaction slows itself down due to a reduced proton diffusion in the already protonated garnets. Compared to the un-protonated garnets, the protonated ones have a much lower Li⁺ conductivity, since a concerted Li–H diffusion mechanism is hindered by the relatively immobile protons. In Li-stuffed garnets like Li₇La₃Zr₂O₁₂ and its doped or substituted derivatives, the LHX preferentially takes place at the 96*h* sites, whereas the 24*d* sites are favored in garnets with low Li content (for instance ≤ 6 pfu). However, due to the large family of garnet materials, the existing experimental studies represent only spotlights on this very broad topic and a comprehensive picture over the full composition/substitutions and structural range as well as various ambient conditions is needed. Future studies using computation methods like modeling and machine learning are suggested here, in order to enable the screening of even more variations.^[48] With a more complete picture, elucidating the influence of dopants and substitutions as well as the Li⁺ or OH⁻ concentration in the aqueous media on LHX even further, a stable water/garnet system can be designed and further improve the sustainability of this promising no-toxic material.

With the aspect of practical processing, it is suggested to have large grain size and less grain boundary content in the garnet-based cell component in order to increase the stability against moisture air. After the final sintering step, the garnet separators would be better to be preserved in dry room or inert-gas protected glovebox for avoiding the adverse effects of LHX. Nevertheless, LHX was shown to be reversible by a high-temperature thermal treatment combined with additional Li sources and is found to be suppressed when garnets are treated in concentrated Li salt or base solutions. Therefore, handling and processing garnet materials in ambient atmosphere and by water-based processing are already feasible options to develop, for example, all-solid-state batteries or aqueous Li-air batteries as future high-energy density storage systems, though the issue of Li dendrite remains challenging especially at high-rate operation. In addition, the tendency to LHX could be used in future recycling strategies, as it could easily leach the Li from

garnet materials in batteries properly designed and prepared for recycling. This way, a sustainable life cycle for future batteries, from materials preparation over cell design and manufacturing all the way to end-of-life and recycling can help to shape a greener future.

Acknowledgements

This work is supported by the Ministry of Economic Affairs, Innovation, Digitalization and Energy of the State NRW, Germany within the project "GrEEn" (No. 313-W044B). R.Y. and N.I. thank Japan Society for the Promotion of Science (JSPS) for the academic exchange within the JSPS Summer Program. Open Access funding enabled and organized by Projekt DEAL.

Conflict of Interest

The authors declare no conflict of interest.

Keywords: batteries · electrochemistry · garnet · lithium proton exchange · solid electrolyte

- [1] a) Y. Ding, Z. P. Cano, A. Yu, J. Lu, Z. Chen, *Electrochem. Energy Rev.* **2019**, *2*, 1–28; b) M. Armand, J. M. Tarascon, *Nature* **2008**, *451*, 652–657; c) T. Placke, R. Kloepsch, S. Dühnen, M. Winter, *J. Solid State Electrochem.* **2017**, *21*, 1939–1964; d) V. Etacheri, R. Marom, R. Elazari, G. Salitra, D. Aurbach, *Energy Environ. Sci.* **2011**, *4*, 3243–3262.
- [2] a) Q. Zhao, S. Stalin, C.-Z. Zhao, L. A. Archer, *Nat. Rev. Mater.* **2020**, *5*, 229–252; b) W. Zhao, J. Yi, P. He, H. Zhou, *Electrochem. Energy Rev.* **2019**; c) Z. H. Gao, H. B. Sun, L. Fu, F. L. Ye, Y. Zhang, W. Luo, Y. H. Huang, *Adv. Mater.* **2018**, *30*, 1705702; d) K. Takada, *J. Power Sources* **2018**, *394*, 74–85; e) F. Zheng, M. Kotobuki, S. Song, M. O. Lai, L. Lu, *J. Power Sources* **2018**, *389*, 198–213; f) A. Manthiram, X. W. Yu, S. F. Wang, *Nat. Rev. Mater.* **2017**, *2*; g) J. Janek, W. G. Zeier, *Nat. Energy* **2016**, *1*, 16141.
- [3] a) C. Wang, K. Fu, S. P. Kammampata, D. W. McOwen, A. J. Samson, L. Zhang, G. T. Hitz, A. M. Nolan, E. D. Wachsman, Y. Mo, V. Thangadurai, L. Hu, *Chem. Rev.* **2020**; b) N. Zhao, W. Khokhar, Z. Bi, C. Shi, X. Guo, L.-Z. Fan, C.-W. Nan, *Joule* **2019**, *3*, 1190–1199; c) P. Albertus, S. Babinec, S. Litzelman, A. Newman, *Nat. Energy* **2018**, *3*, 16–21; d) S. Ramakumar, C. Deviannapoorani, L. Dhivya, L. S. Shankar, R. Murugan, *Prog. Mater. Sci.* **2017**, *88*, 325–411; e) C.-L. Tsai, S. Yu, H. Tempel, H. Kungl, R.-A. Eichel, *Mater. Technol.* **2020**, *35*, 656–674.
- [4] a) M. Ihrig, M. Finsterbusch, C.-L. Tsai, A. M. Laptev, C.-h. Tu, M. Bram, Y. J. Sohn, R. Ye, S. Sevinc, S.-k. Lin, D. Fattakhova-Rohlfing, O. Guillon, *J. Power Sources* **2021**, *482*, 228905; b) M. Rosen, R. Ye, M. Mann, S. Lobe, M. Finsterbusch, O. Guillon, D. Fattakhova-Rohlfing, *J. Mater. Chem. A* **2021**, *9*, 4831–4840.
- [5] H. Huo, J. Luo, V. Thangadurai, X. Guo, C.-W. Nan, X. Sun, *ACS Energy Lett.* **2020**, *5*, 252–262.
- [6] a) H. Duan, H. Zheng, Y. Zhou, B. Xu, H. Liu, *Solid State Ionics* **2018**, *318*, 45–53; b) K. Hofstetter, A. J. Samson, S. Narayanan, V. Thangadurai, *J. Power Sources* **2018**, *390*, 297–312.
- [7] V. Thangadurai, H. Kaack, W. J. F. Weppner, *J. Am. Ceram. Soc.* **2003**, *86*, 437–440.
- [8] V. Thangadurai, W. Weppner, *Adv. Funct. Mater.* **2005**, *15*, 107–112.
- [9] R. Murugan, V. Thangadurai, W. Weppner, *Angew. Chem. Int. Ed.* **2007**, *46*, 7778–7781; *Angew. Chem.* **2007**, *119*, 7925–7928.
- [10] a) A. J. Samson, K. Hofstetter, S. Bag, V. Thangadurai, *Energy Environ. Sci.* **2019**, *12*, 2957–2975; b) Y. Li, J.-T. Han, C.-A. Wang, H. Xie, J. B. Goodenough, *J. Mater. Chem.* **2012**, *22*, 15357–15361; c) V. Thangadurai, S. Narayanan, D. Pinzaru, *Chem. Soc. Rev.* **2014**, *43*, 4714–4727.
- [11] a) A. Sharafi, E. Kazyak, A. L. Davis, S. Yu, T. Thompson, D. J. Siegel, N. P. Dasgupta, J. Sakamoto, *Chem. Mater.* **2017**, *29*, 7961–7968; b) A. Sharafi, S. Yu, M. Naguib, M. Lee, C. Ma, H. M. Meyer, J. Nanda, M. Chi, D. J.

- Siegel, J. Sakamoto, *J. Mater. Chem. A* **2017**, *5*, 13475–13487; c) L. Cheng, C. H. Wu, A. Jarry, W. Chen, Y. Ye, J. Zhu, R. Kostecki, K. Persson, J. Guo, M. Salmeron, G. Chen, M. Doeff, *ACS Appl. Mater. Interfaces* **2015**, *7*, 17649–17655; d) L. Cheng, E. J. Crumlin, W. Chen, R. Qiao, H. Hou, S. Franz Lux, V. Zorba, R. Russo, R. Kostecki, Z. Liu, K. Persson, W. Yang, J. Cabana, T. Richardson, G. Chen, M. Doeff, *Phys. Chem. Chem. Phys.* **2014**, *16*, 18294–18300; e) L. Cheng, J. S. Park, H. M. Hou, V. Zorba, G. Y. Chen, T. Richardson, J. Cabana, R. Russo, M. Doeff, *J. Mater. Chem. A* **2014**, *2*, 172–181; f) W. Xia, B. Xu, H. Duan, Y. Guo, H. Kang, H. Li, H. Liu, *ACS Appl. Mater. Interfaces* **2016**, *8*, 5335–5342.
- [12] W. Xia, B. Xu, H. Duan, X. Tang, Y. Guo, H. Kang, H. Li, H. Liu, *J. Am. Ceram. Soc.* **2017**, *100*, 2832–2839.
- [13] a) M. Nyman, T. M. Alam, S. K. McIntyre, G. C. Bleier, D. Ingersoll, *Chem. Mater.* **2010**, *22*, 5401–5410; b) C. Galven, J. Dittmer, E. Suard, F. Le Berre, M.-P. Crosnier-Lopez, *Chem. Mater.* **2012**, *24*, 3335–3345; c) L. Truong, J. Colter, V. Thangadurai, *Solid State Ionics* **2013**, *247*, 1–7; d) H. Nemori, Y. Matsuda, S. Mitsuda, M. Matsui, O. Yamamoto, Y. Takeda, N. Imanishi, *Solid State Ionics* **2015**, *282*, 7–12; e) L. Truong, V. Thangadurai, *Inorg. Chem.* **2012**, *51*, 1222–1224.
- [14] a) C. Galven, E. Suard, D. Mounier, M.-P. Crosnier-Lopez, F. Le Berre, *J. Mater. Res.* **2013**, *28*, 2147–2153; b) K. Hofstetter, A. J. Samson, V. Thangadurai, *Solid State Ionics* **2018**, *318*, 71–81.
- [15] a) R. Ye, C.-L. Tsai, M. Ihrig, S. Sevinc, M. Rosen, E. Dashjav, Y. J. Sohn, E. Figgemeier, M. Finsterbusch, *Green Chem.* **2020**, *22*, 4952b) Z. F. Yow, Y. L. Oh, W. Y. Gu, R. P. Rao, S. Adams, *Solid State Ionics* **2016**, *292*, 122–129; c) C. Liu, K. Rui, C. Shen, M. E. Badding, G. X. Zhang, Z. Y. Wen, *J. Power Sources* **2015**, *282*, 286–293; d) C. Galven, J.-L. Fourquet, M.-P. Crosnier-Lopez, F. Le Berre, *Chem. Mater.* **2011**, *23*, 1892–1900; e) C. Ma, E. Rangasamy, C. Liang, J. Sakamoto, K. L. More, M. Chi, *Angew. Chem. Int. Ed.* **2015**, *54*, 1063–1063; *Angew. Chem.* **2015**, *127*, 1077–1077; f) A. Orera, G. Larraz, J. A. Rodríguez-Velamazán, J. Campo, M. L. Sanjuán, *Inorg. Chem.* **2016**, *55*, 1324–1332.
- [16] Y. Li, J.-T. Han, S. C. Vogel, C.-A. Wang, *Solid State Ionics* **2015**, *269*, 57–61.
- [17] C. Hiebl, D. Young, R. Wagner, H. M. R. Wilkening, G. J. Redhammer, D. Rettenwander, *J. Phys. Chem. C* **2019**, *123*, 1094–1098.
- [18] F. Gam, C. Galven, A. Bulou, F. Le Berre, M.-P. Crosnier-Lopez, *Inorg. Chem.* **2014**, *53*, 931–934.
- [19] R. Kun, F. Langer, M. Delle Piane, S. Ohno, W. G. Zeier, M. Gockeln, L. C. Ciacchi, M. Busse, I. Fekete, *ACS Appl. Mater. Interfaces* **2018**, *10*, 37188–37197.
- [20] L. Truong, V. Thangadurai, *Chem. Mater.* **2011**, *23*, 3970–3977.
- [21] G. J. Redhammer, P. Badami, M. Meven, S. Ganschow, S. Berendts, G. Tippelt, D. Rettenwander, *ACS Appl. Mater. Interfaces* **2021**, *12*, 350–359.
- [22] X. M. Liu, Y. Chen, Z. D. Hood, C. Ma, S. H. Yu, A. Sharafi, H. Wang, K. An, J. Sakamoto, D. J. Siegel, Y. Q. Cheng, N. H. Jalarvo, M. F. Chi, *Energy Environ. Sci.* **2019**, *12*, 945–951.
- [23] M. L. Sanjuán, A. Orera, I. Sobrados, A. F. Fuentes, J. Sanz, *J. Mater. Chem. A* **2018**, *6*, 2708–2720.
- [24] G. Larraz, A. Orera, M. L. Sanjuán, *J. Mater. Chem. A* **2013**, *1*, 11419–11428.
- [25] M. Matsui, K. Takahashi, K. Sakamoto, A. Hirano, Y. Takeda, O. Yamamoto, N. Imanishi, *Dalton Trans.* **2014**, *43*, 1019–1024.
- [26] a) S. Toda, K. Ishiguro, Y. Shimonishi, A. Hirano, Y. Takeda, O. Yamamoto, N. Imanishi, *Solid State Ionics* **2013**, *233*, 102–106; b) I. Quinzeni, D. Capsoni, V. Berbenni, P. Mustarelli, M. Sturini, M. Bini, *Mater. Chem. Phys.* **2017**, *185*, 55–64.
- [27] S. Uhlenbruck, C. Dellen, S. Moller, S. Lobe, C. L. Tsai, M. Finsterbusch, M. Bram, O. Guillon, *Solid State Ionics* **2018**, *320*, 259–265.
- [28] S. Ohta, M. Kawakami, H. Nozaki, C. Yada, T. Saito, H. Iba, *J. Mater. Chem. A* **2020**, *8*, 8989–8996.
- [29] a) Y. Shimonishi, A. Toda, T. Zhang, A. Hirano, N. Imanishi, O. Yamamoto, Y. Takeda, *Solid State Ionics* **2011**, *183*, 48–53; b) K. Ishiguro, H. Nemori, S. Sunahiro, Y. Nakata, R. Sudo, M. Matsui, Y. Takeda, O. Yamamoto, N. Imanishi, *J. Electrochem. Soc.* **2014**, *161*, A668–A674; c) S. Narayanan, F. Ramezanipour, V. Thangadurai, *Inorg. Chem.* **2015**, *54*, 6968–6977.
- [30] L. Cheng, M. Liu, A. Mehta, H. Xin, F. Lin, K. Persson, G. Chen, E. J. Crumlin, M. Doeff, *ACS Appl. Energy Mater.* **2018**, *1*, 7244–7252.
- [31] J. Cai, B. Polzin, L. Fan, L. Yin, Y. Liang, X. Li, Q. Liu, S. E. Trask, Y. Liu, Y. Ren, X. Meng, Z. Chen, *Mater. Today* **2021**, 100669.
- [32] M. Wood, X. Gao, R. Shi, T. W. Heo, J. A. Espitia, E. B. Duoss, B. C. Wood, J. Ye, *J. Power Sources* **2021**, *484*, 229252.
- [33] S. Dühnen, J. Betz, M. Kolek, R. Schmich, M. Winter, T. Placke, *Small Methods* **2020**, *4*, 2000039.
- [34] X. Huang, Y. Lu, J. Tin, S. Gu, T. P. Xiu, Z. Song, M. E. Badding, Z. Y. Wen, *ACS Appl. Mater. Interfaces* **2018**, *10*, 17147–17155.
- [35] X. Peng, X. K. Zhang, K. Huang, S. P. Song, Y. Xiang, *ChemElectroChem* **2019**, *6*, 2945–2948.
- [36] R. A. Jonson, E. Yi, F. Shen, M. C. Tucker, *Energy Fuels* **2021**, *35*, 8982–8990.
- [37] a) L. Buannic, M. Naviroj, S. M. Miller, J. Zagorski, K. T. Faber, A. Llordes, J. Am. Ceram. Soc. **2019**, *102*, 1021–1029; b) H. Shen, E. Yi, M. Amores, L. Cheng, N. Tamura, D. Y. Parkinson, G. Chen, K. Chen, M. Doeff, *J. Mater. Chem. A* **2019**, *7*, 20861–20870; c) H. Shen, E. Yi, S. Heywood, D. Y. Parkinson, G. Chen, N. Tamura, S. Sofie, K. Chen, M. M. Doeff, *ACS Appl. Mater. Interfaces* **2020**, *12*, 3494–3501; d) E. Yi, H. Shen, S. Heywood, J. Alvarado, D. Y. Parkinson, G. Chen, S. W. Sofie, M. M. Doeff, *ACS Appl. Energy Mater.* **2020**, *3*, 170–175.
- [38] a) L. Miara, A. Windmuller, C. L. Tsai, W. D. Richards, Q. L. Ma, S. Uhlenbruck, O. Guillon, G. Ceder, *ACS Appl. Mater. Interfaces* **2016**, *8*, 26842–26850; b) L. J. Miara, W. D. Richards, Y. E. Wang, G. Ceder, *Chem. Mater.* **2015**, *27*, 4040–4047.
- [39] X. Wang, J. Wang, F. Li, F. Zhu, C. Ma, *Ceram. Int.* **2020**, *46*, 18544–18550.
- [40] a) M. Cai, J. Jin, Z. Wen, *Acta Phys. Chim. Sin.* **2021**, *37*, 2009006; b) M. Cai, Y. Lu, L. Yao, J. Jin, Z. Wen, *Chem. Eng. J.* **2021**, *417*, 129158; c) M. Cai, Y. Lu, J. Su, Y. Ruan, C. Chen, B. V. R. Chowdari, Z. Wen, *ACS Appl. Mater. Interfaces* **2019**, *11*, 35030–35038.
- [41] H. Huo, Y. Chen, N. Zhao, X. Lin, J. Luo, X. Yang, Y. Liu, X. Guo, X. Sun, *Nano Energy* **2019**, *61*, 119–125.
- [42] a) Y. D. Ruan, Y. Lu, X. Huang, J. M. Su, C. Z. Sun, J. Jin, Z. Y. Wen, *J. Mater. Chem. A* **2019**, *7*, 14565–14574; b) H. Duan, W.-P. Chen, M. Fan, W.-P. Wang, L. Yu, S.-J. Tan, X. Chen, Q. Zhang, S. Xin, L.-J. Wan, Y.-G. Guo, *Angew. Chem. Int. Ed.* **2020**, *59*, 12069–12075; *Angew. Chem.* **2020**, *132*, 12167–12173.
- [43] Y. Ruan, Y. Lu, Y. Li, C. Zheng, J. Su, J. Jin, T. Xiu, Z. Song, M. E. Badding, Z. Wen, *Adv. Funct. Mater.* **2021**, *31*, 2007815.
- [44] a) Y. Wang, J. Yi, Y. Xia, *Adv. Energy Mater.* **2012**, *2*, 830–840; b) A. Manthiram, L. Li, *Adv. Energy Mater.* **2015**, *5*, 1401302.
- [45] N. Imanishi, M. Matsui, Y. Takeda, O. Yamamoto, *Electrochemistry* **2014**, *82*, 938–945.
- [46] K. Liu, C.-A. Wang, *Electrochem. Commun.* **2014**, *48*, 147–150.
- [47] C. Zhan, K. Zhang, Y. Li, M. Zhang, Z. Shen, *Electrochim. Acta* **2020**, *343*, 136163.
- [48] X. Chen, X. Liu, X. Shen, Q. Zhang, *Angew. Chem. Int. Ed.* DOI: 10.1002/anie.202107369; *Angew. Chem.* DOI: 10.1002/ange.202107369.

Manuscript received: June 6, 2021

Revised manuscript received: July 7, 2021

Accepted manuscript online: July 15, 2021

Version of record online: August 5, 2021